Available online at www.sciencedirect.com

ScienceDirect

Ceramics International 39 (2013) 8657–8666

CERAMICS INTERNATIONAL

www.elsevier.com/locate/ceramint

Mechanochemical synthesis and structural characterization of nano-sized amorphous tricalcium phosphate

Bahman Nasiri-Tabrizi*, Abbas Fahami

Materials Engineering Department, Najafabad Branch, Islamic Azad University, Najafabad, Isfahan, Iran

Received 4 March 2013; received in revised form 8 April 2013; accepted 11 April 2013
Available online 19 April 2013

Abstract

Nano-sized amorphous tricalcium phosphate powders were synthesized through different mechanochemical reactions. The influence of milling parameters and chemical composition of reagents on the formation of amorphous tricalcium phosphate was investigated. In all the experiments, the mole ratio of calcium to phosphorous oxide was 3:1, i.e. the stoichiometric Ca/P content in the composition of amorphous tricalcium phosphate (Ca/P = 1.5). Results revealed that the phase purity, structural features, and morphological characteristics of products were significantly influenced by the chemical composition of raw materials and milling parameters. For all the reactions, amorphous tricalcium phosphate was formed as the main product of mechanical activation after 10 h. After annealing at 1100 °C, crystallization of amorphous phase occurred, and consequently high crystalline β-tricalcium phosphate was generated. According to FT-IR findings, the synthesized powders had high chemical purity. After 10 h of milling, the obtained nanopowders through four distinct reactions exhibited crystallite sizes about 20, 69, 58 and 55 nm. The results from scanning electron micrographs showed that the mean size of agglomerate was in the range of 1–5 μm. Detailed study of morphological features by using transmission electron microscopy confirmed the formation of nano-sized amorphous tricalcium phosphate with spheroidal and ellipse-like morphologies.

Keywords: Nano-sized; Amorphous tricalcium phosphate; Mechanochemical; Structural features

1. Introduction

Amorphous calcium phosphate (ACP) phases are one of the most frequent forms of calcium phosphate minerals in biological organisms. These biomaterials play a crucial role in several biomedical applications. They have been found, for instance, in the mitochondria of eukaryote and prokaryote cells and is also considered as a precursor phase of bone mineral in vertebrates. ACP is present in many biomaterials and preparations, for example, in coatings of metallic endoprostheses as a transitory phase, in self-setting injectable cements as responsible for the setting reaction, in composite materials as a remineralising phase for enamel and dentine, and in toothpaste formulations as a remineralising agent for early carious lesions [1–3].

According to the literature [4], various amorphous calcium phosphates (ACPs) have been distinguished only by Ca/P ratio. Amorphous tricalcium phosphate (ATCP), with an atomic Ca/P ratio of 1.5 and the chemical formula $Ca_3(PO_4)_2 \cdot xH_2O$, is most widely found in amorphous precipitates obtained in alkaline media (pH range 9–11) [4]. It has been found that in the absence of mineral ions other than Ca^{2+} and PO_4^{3-} the composition of ACP is restrained to the mentioned chemical formula for charge balance reasons [1]. In the more acidic solutions, ACPs can contain HPO_4^{2-} ions instead of PO_4^{3-}, leading to a lower Ca/P ratio. However, such phases are unstable and convert very rapidly into dicalcium phosphate dihydrate (DCPD, $CaHPO_4 \cdot 2H_2O$). In addition, in non-aqueous or ethanol–water media ACPs with a much lower Ca/P ratio than composition of ATCP can be obtained that corresponds to amorphous octacalcium phosphate (AOCP, $Ca_8H_2(PO_4)_4 \cdot xH_2O$) or amorphous dicalcium phosphate (ADCP, $CaHPO_4$) [5–7]. Also, ACPs with a Ca/P ratio higher than 1.5 can only be obtained in the presence of foreign ions, most frequently carbonate and oxide ions. It should be noted that the composition of ATCP can change on ageing due to the internal hydrolysis. The hydrolysis process led to a range of compositions represented as: $Ca_9(PO_4)_{6-x}(HPO_4)_x(OH)_x$ [8]. In general, ACPs can be

*Corresponding author. Tel.: +98 3114456551; fax: +98 3312291008.
E-mail address: bahman_nasiri@hotmail.com (B. Nasiri-Tabrizi).

0272-8842/$ - see front matter © 2013 Elsevier Ltd and Techna Group S.r.l. All rights reserved.
http://dx.doi.org/10.1016/j.ceramint.2013.04.045

synthesized by two main routes which include wet route (in aqueous medium at low temperature) and dry process (using high energy processing or high temperature) [9–18]. Depending on the method of the formation and experimental circumstances, the outcomes can show a Ca/P ratio ranging from 1 to 2 or even higher. It has been reported that the wet synthesis route of ACP is based on the double decomposition of a calcium and phosphate salt in aqueous or water–alcohol solutions [1,3,8]. In addition to the aforementioned wet procedures, various types of ACPs can be synthesized by dry processes [14–17]. In a different approach, a crystalline to amorphous transition has been detected for various calcium orthophosphates at very high (upto 10 GPa) pressures [18].

Although the various types of ACPs have been produced by several researchers in different conditions [9–18], synthesis and characterization of nano-sized amorphous tricalcium phosphates (n-ATCPs) are still a much-discussed question [19]. The basic structural units of ATCP are roughly spherical clusters which randomly packed in spherical particles with water in the interstices [19,20]. However, several details in mechanosynthesis of n-ATCPs still remain unclear. Therefore, the main purpose of this study was to analyze the structural and morphological features of n-ATCPs obtained under different mechanochemical reactions. In fact, the effect of milling parameters (time and media) and chemical composition of reagents on the formation of n-ATCP was investigated. In addition, the phase transformation during thermal annealing process was examined.

2. Materials and methods

Analytical grade calcium hydroxide ($Ca(OH)_2$, Fluka), anhydrous dicalcium phosphate ($CaHPO_4$, Merck), calcium oxide (CaO, Merck), and phosphorous pentoxide (P_2O_5, Merck) were used as precursor materials for the preparation of n-ATCP through four distinct mechanochemical processes. In all the reactions, the ratio of calcium to phosphorous oxide was 3:1 (mole ratio), i.e. the stoichiometric Ca/P content in the composition of amorphous tricalcium phosphate (ATCP: Ca/P=1.5). The weight ratio of ball-to-powder, total powder mass and rotational speed used in each preparation were 20:1, 6 g and 600 rpm, respectively. The objectives of mechanical activation were twofold: to evaluate the effect of milling parameters on the formation of n-ATCP and to appraise the influence of chemical composition of raw materials on the mechanosynthesis of n-ATCP. For the first aim, the powder mixtures consisting of CaO and P_2O_5 were ground on a planetary ball mill using two distinct milling media. The first media was composed of sealed tempered chrome steel vial (vol. 125 ml) and balls (20 mm in diameter). The second media was comprised of sealed tempered chrome steel (vol. 125 ml) and un-fused alumina balls (diameter 20 mm). Milling was carried out for 1, 5, and 10 h in both the milling media under air atmosphere. The milling conditions in the first and second media were named as M1 and M2, respectively. For the second object, four distinct chemical reactions were mechanically activated for 10 h using sealed tempered chrome steel vials and balls. These mechanochemical procedures are as follows:

$$3CaO+P_2O_5 \rightarrow Ca_3(PO_4)_2 \cdot xH_2O \quad \text{(Activated under air atmosphere, Ca/P=1.5)} \tag{1}$$

$$CaO+2CaHPO_4 \rightarrow Ca_3(PO_4)_2 \cdot xH_2O \quad \text{(Activated under air atmosphere, Ca/P=1.5)} \tag{2}$$

$$3Ca(OH)_2+P_2O_5 \rightarrow Ca_3(PO_4)_2 \cdot xH_2O \quad \text{(Activated under air atmosphere, Ca/P=1.5)} \tag{3}$$

$$Ca(OH)_2+2CaHPO_4 \rightarrow Ca_3(PO_4)_2 \cdot xH_2O \quad \text{(Activated under air atmosphere, Ca/P=1.5)} \tag{4}$$

The presented reactions from (1) to (4), were named as R1, R2, R3 and R4, respectively. Details of milling conditions and composition of powder mixtures are shown in Fig. 1. To evaluate the effect of thermal treatment on the phase transformation, the milled powder for 10 h was filled in a quartz boat, and then heat treated under atmospheric pressure at 1100 °C for 1 h. The heating rate from room temperature up to the desired temperature was fixed at 10 °C min^{-1}.

Phase evolution and structural features of the outcomes were investigated by X-ray diffraction (Philips X-ray diffractometer (XRD), Cu-K_α radiation, 40 kV, 30 mA and 0.02°S^{-1} step scan). All measurements were conducted at room temperature of 25 °C and with the diffraction range of $20^\circ \leq 2\theta \leq 70^\circ$ at scan speed of 1° min^{-1}. "*PANalytical X'Pert HighScore*" software was utilized for the analysis of different peaks. The XRD patterns were compared to standards compiled by the Joint Committee on Powder Diffraction and Standards (JCPDS), which involved card #018-0303 for $Ca_3(PO_4)_2.xH_2O$, #037-1497 for CaO, #033-0297 for $Ca_2P_2O_7$, #043-1484 for Al_2O_3, and #09-0169 for β-TCP.

The crystallite size and lattice strain of the samples were determined by using the XRD data according to the following equation [21]:

$$B\cos\theta = \frac{0.9\lambda}{D} + \eta \sin\theta \tag{I}$$

where λ, D, η and θ are the wavelength of the X-ray used (0.154056 nm), crystallite size, lattice strain and the Bragg angle (°), respectively. Note that B in the above equation is the peak width (in radians) after subtracting the peak width due to instrumental broadening from the experimentally recorded

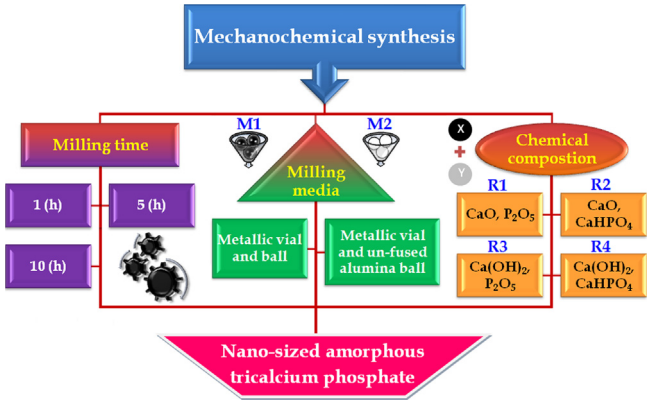

Fig. 1. Details of milling conditions and composition of powder mixtures.

profile. Thus, when $B\cos\theta$ is plotted against $\sin\theta$, a straight line is obtained with the slope as η and the intercept as $0.9\,\lambda/D$.

Moreover, the volume fraction of grain boundary, f, is approximately [22]:

$$f = 1-\left[\frac{D}{(D+t)}\right]^3 \quad \text{(II)}$$

where D and t are diameter of a spherical crystallite and a shell of grain boundary, respectively. Values of f were calculated from this equation by substituting the experimental crystallite size obtained by XRD with D under the assumption of $t=1$ nm.

Crystallinity degree (X_c), corresponding to the fraction of crystalline phase present in the examined volume, was estimated for the synthesized samples by taking the sum total of relative intensities of individual characteristic peaks according to the following equation [23]:

$$X_C = \frac{\text{Sum total of relative intensities of ATCP}}{\text{Sum total of relative intensities of standard}} \times 100 \quad \text{(III)}$$

The functional groups of products were measured using Fourier transformed infrared (FT-IR) transmission spectroscopy (Perkin-Elmer Spectrum 65 FT-IR Spectrometer, USA) in the range 4000–400 cm^{-1} with the resolution of 2 cm^{-1}. For FT-IR analysis, the crushed samples were diluted 100 fold with KBr powder and the background noise was corrected with pure KBr data. Morphological characteristics of the synthesized powders were determined on a scanning electron microscope (LEO 435VP, LEO Electron Microscopy Ltd., Cambridge, UK). Also, the size and morphology of fine powders were observed on a transmission electron microscope (Philips CM10, Eindhoven, The Netherlands) that operated at the acceleration voltage of 100 kV.

3. Results and discussion

3.1. Effect of milling parameters (milling time and media type)

Fig. 2 shows the XRD patterns of CaO and P_2O_5 powder mixture after mechanical activation for different milling times (1–10 h) in both the milling media. Phosphoric acid was formed immediately after the addition of P_2O_5 to the reaction mixture owing to its hygroscopic nature.

$$P_2O_5 + 3H_2O \rightarrow 2H_3PO_4 \quad (5)$$

After 1 h of milling, a quantity of CaO transformed to Ca $(OH)_2$ due to the mechanical activation under air atmosphere. Simultaneously, calcium hydroxide and phosphoric acid reacted at ambient temperature and led to the formation of calcium pyrophosphate. It can be seen that the phase compositions were CaO and $Ca_2P_2O_7$ after 1 h of milling. In M1 media, when the mechanical activation time was extended to 5 h, several characteristic peaks corresponding to CaO and $Ca_2P_2O_7$ disappeared and a poorly crystallized structure was formed. The poorly crystallized phase is believed to be a amorphous tricalcium phosphate ($Ca_3(PO_4)_2\cdot xH_2O$), which is supported by the Ca/P ratio of 1.5. Further increasing the activation time to 10 h caused a further decrease in the fraction of crystalline phase, as evidenced by the extra broadening of the principal diffraction peaks. After 10 h of milling, similar to the previous sample, the main product of mechanical activation was $Ca_3(PO_4)_2\cdot xH_2O$. In this profile, few extra peaks were also observed. It suggests that $Ca_2P_2O_7$ and CaO are still present in this sample. In the case of M2 media, similar to M1, amorphous tricalcium phosphate was the dominant phase after 5 h of milling. However, characteristic peaks of the $Ca_2P_2O_7$ and Al_2O_3 were also evident. The presence of Al_2O_3 as an extra phase indicates the adhesion of un-fused alumina balls to

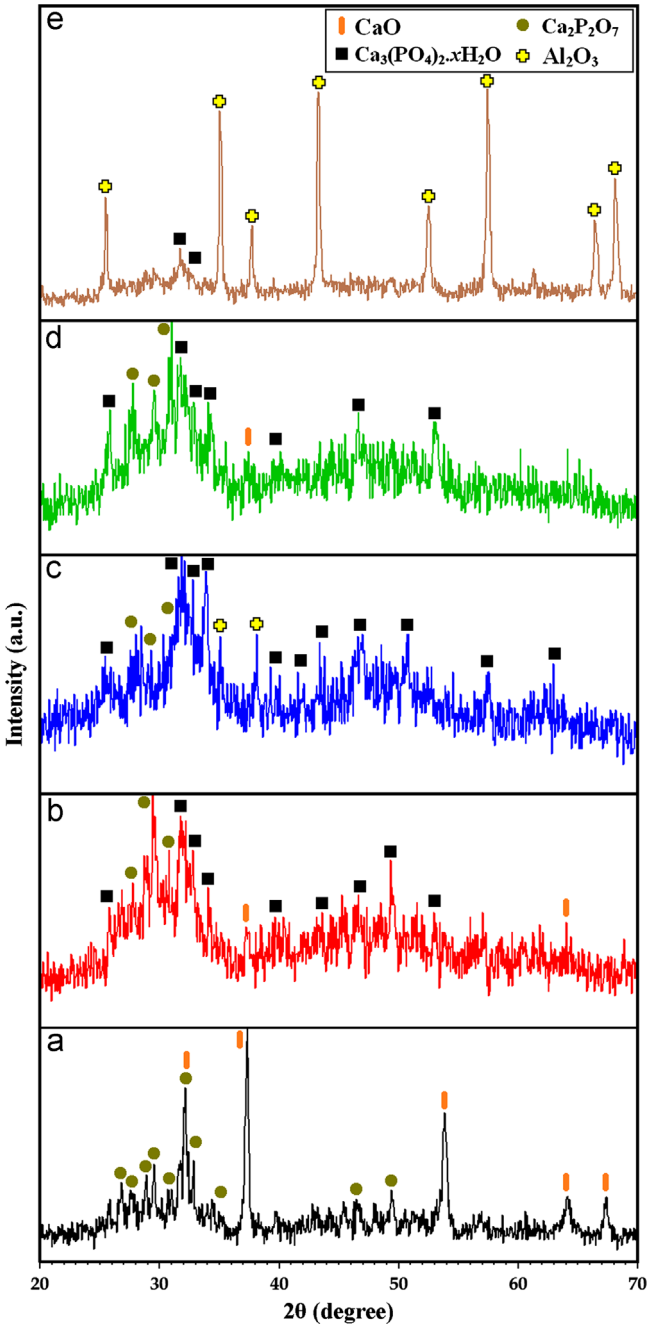

Fig. 2. XRD patterns of CaO and P_2O_5 powder mixture after mechanical activation for different milling times (1–10 h) in both milling media under air atmosphere; (a) 1 h, (b) 5 h in M1, (c) 5 h in M2, (d) 10 h in M1, and (e) 10 h in M2.

the milling media. In this media, increasing milling time to 10 h led to the formation of large quantities of Al_2O_3 due to the excessive adhesion of balls to the milling media. According to XRD profile of this sample, the high crystalline Al_2O_3 was the dominant phase along with minor amount of amorphous tricalcium phosphate. Recalling from the above results, to appraise the influence of chemical composition of raw materials on the mechanosynthesis of n-ATCP only M1 media was served.

3.2. Effect of chemical composition

Fig. 3 shows the XRD patterns of R1, R2, R3 and R4 after 10 h of mechanical activation in M1 media. It can be seen that after 10 h the main product of milling was amorphous tricalcium phosphate. According to XRD profile of the R1, $Ca_2P_2O_7$ and CaO as extra phases were also observed in the sample. It seems that the presence of these extra phases could be a trace of the original product of the R1. So, it can be concluded that the synthesized powder using R1 reaction had the Ca/P ratio lower than stoichiometry value as a result of $Ca_2P_2O_7$ formation after 10 h of milling. Conversely, the obtained powders out of R2, R3 and R4 showed a single ATCP phase without any extra phase after 10 h of milling. This result indicates that the phase purity of mechanosynthesized amorphous tricalcium phosphate is influenced by the chemical composition of raw materials. Based on XRD results, the use of the R2, R3 and R4 is preferred to R1 in order to produce n-ATCP with higher phase purity.

3.3. Structural features

Fig. 4 displays the effect of chemical composition of raw materials on the structural evolution, crystallite size, lattice strain, and volume fraction of grain boundaries of n-ATCP after 10 h of mechanical activation in M1 media. The calculated profiles of the samples in comparison with experimental data in the range of 22° to 30° are shown in Fig. 4a. This approach was applied to monitor the structural evolution of the samples during the milling process. Based on this figure, it can be seen that mechanical activation up to 10 h led to the more line broadening of XRD patterns which confirmed the formation of poorly crystallized phase. However, among the samples, the level of peak broadening in R1 profile was higher than the other specimens due to the large amount of strain imparted to particles during the mechanical activation. In this sample, the peak broadening was accompanied by a drastic decrease in the intensity of peaks. As shown in Fig. 4b, the crystallite size of n-ATCP out of R1, R2, R3 and R4 was around 20, 69, 58 and 55 nm after 10 h of milling, respectively. Also, the lattice strain of n-ATCP was about 0.83% for R1, 0.57% for R2, 0.64% for R3, and 0.65% for R4. It should be noted that the volume fraction of grain boundary of n-ATCP out of R1, R2, R3 and R4 was around 13.61%, 4.22%, 4.99% and 5.26%, respectively. Comparison of the obtained results revealed that the synthesized powders out of R1 had minimum value of crystallite size. In opposition, the

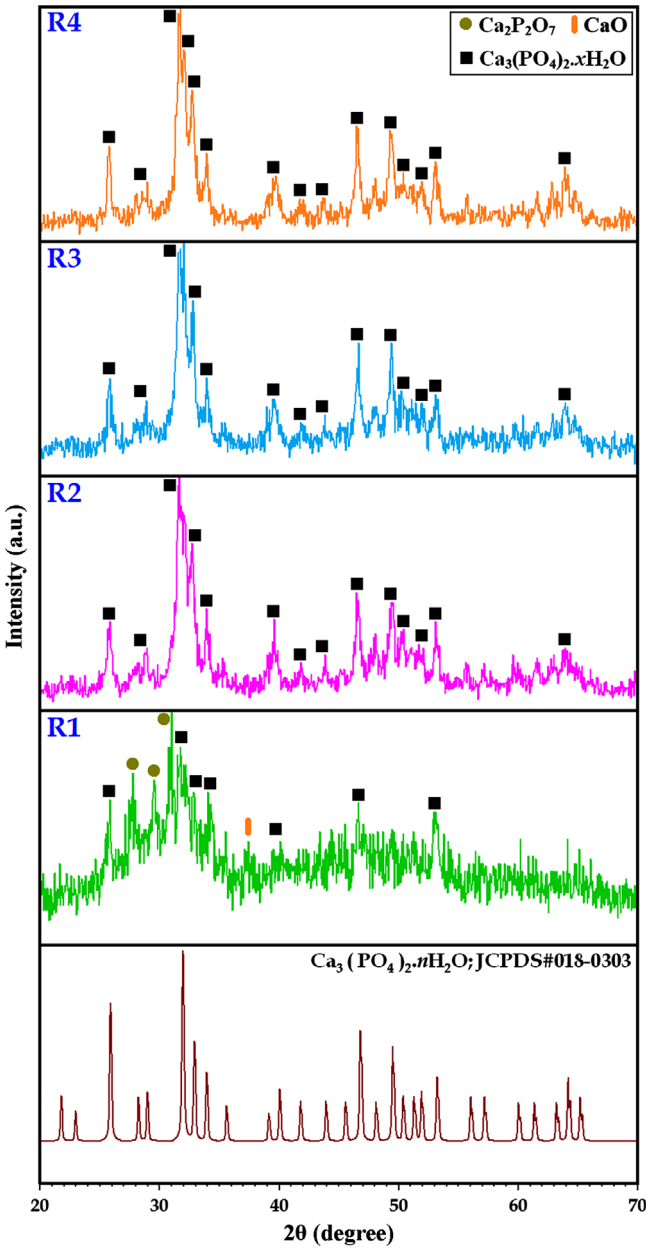

Fig. 3. XRD patterns of R1, R2, R3 and R4 after 10 h of mechanical activation in M1 media.

maximum amount of lattice strain and volume fraction of grain boundary of n-ATCP belonged to R1 and the minimum values were related to the R2.

Fig. 5 displays the crystallinity degree of the samples (X_c) as the function of milling time and chemical composition of raw materials. According to Fig. 5a, in M1 media, the crystallinity was about 62% and 22% after 5 and 10 h of milling, respectively. In the case of M2 media, the crystallinity was about 50% after 5 h of milling. With increasing milling time to 10 h, crystallinity decreased and reached a minimum (2%). These results indicate that the crystallinity of n-ATCP is significantly influenced by the milling time and media type. On the other hand, in accordance with Fig. 5b, it can be seen that the crystallinity was also clearly influenced by the chemical

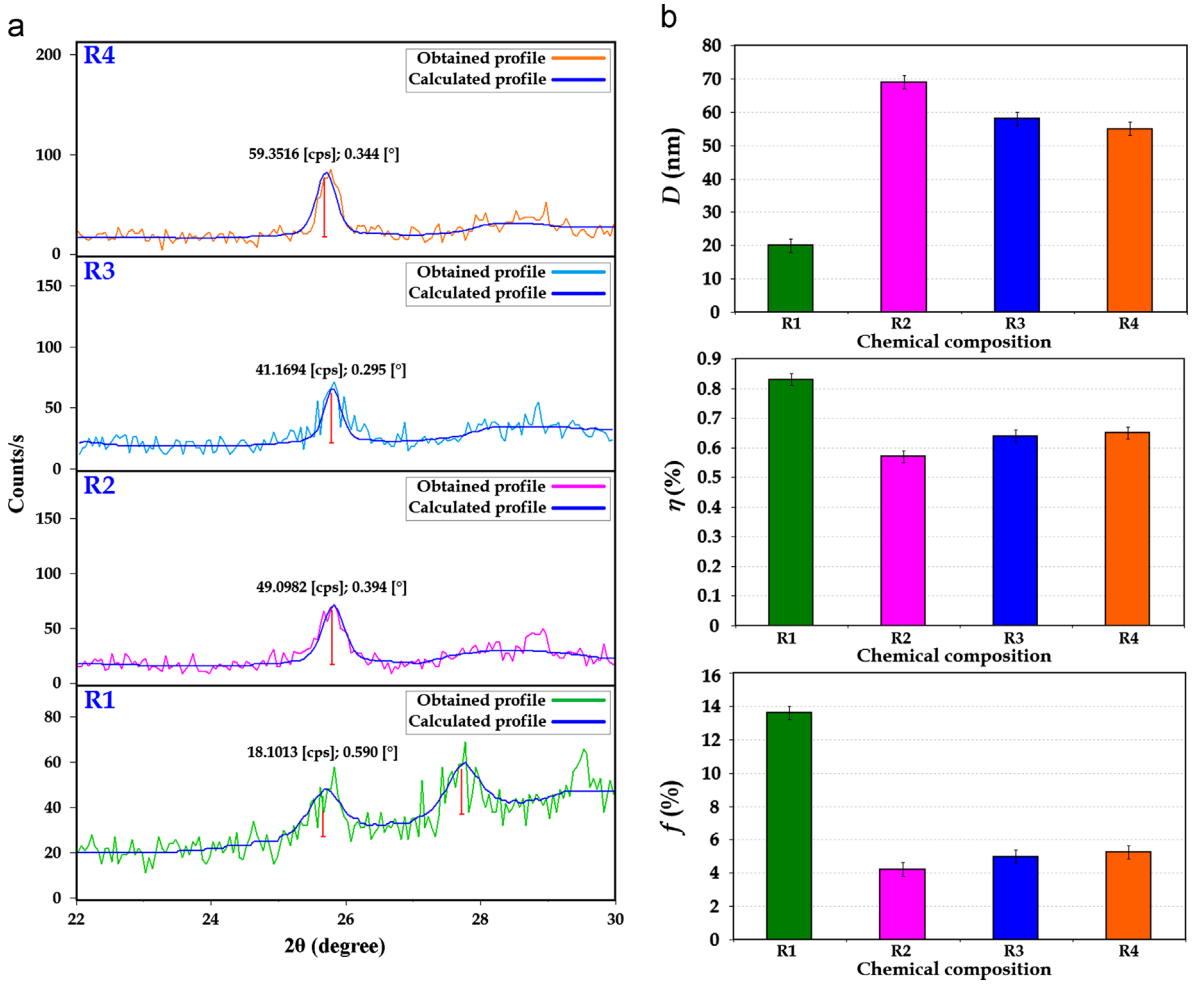

Fig. 4. The effect of chemical composition of raw materials on the (a) structural evolution, (b) crystallite size, volume fraction of grain boundaries and lattice strain of n-ATCP after 10 h of mechanical activation in M1 media.

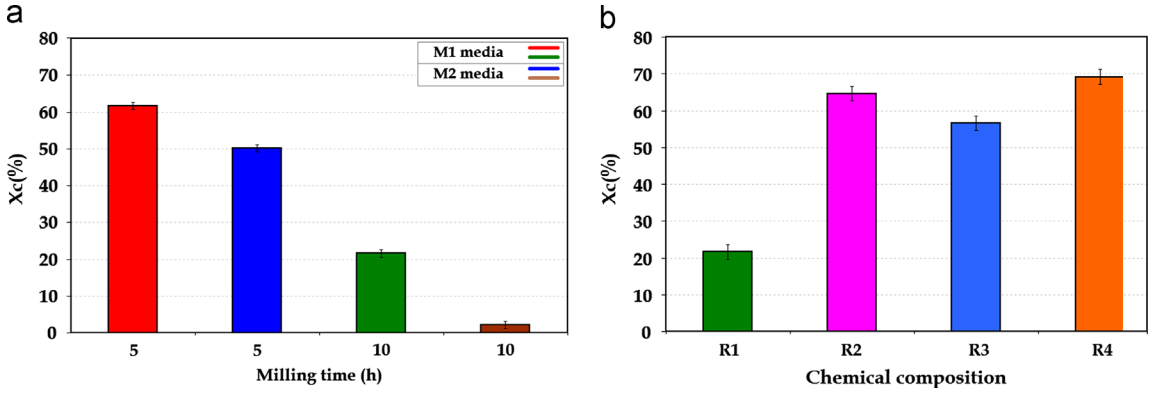

Fig. 5. The crystallinity degree of the samples (X_c) as the function of: (a) milling time and (b) chemical composition of raw materials.

composition of raw materials. So, the degree of crystallinity was not the same for different reactions. Comparison of these results revealed that the obtained powders out of R1 and R4 had minimum and maximum degree of crystallinity, respectively. It has been found that the control of the crystallinity of calcium phosphates is necessary for their biological applications [24]. Since low-level crystallinity of calcium phosphates shows high osteoconductivity, the synthesized powders can be used to promote osseointegration or as a coating to promote bone ingrowth in to prosthetic implants [25].

3.4. Evaluation of functional groups (FT-IR analysis)

Fig. 6 shows the FT-IR spectra of R1, R2, R3 and R4 after 10 h of mechanical activation in M1 media. It has been reported that [26–29], the functional groups generally observed

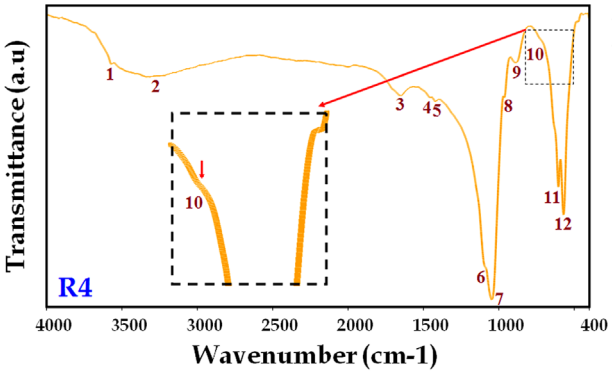

No.	cm^{-1}	Assignment	No.	cm^{-1}	Assignment
1	3570.8	OH^-	7	1046.19	$\nu_3(PO_4^{3-})$
2	3312.52	H_2O	8	965.5	$\nu_3(PO_4^{3-})$
3	1652.2	H_2O	9	884.71	CO_3^{2-}
4	1460.3	CO_3^{2-}	10	729.72	$P_2O_7^{4-}$
5	1420	CO_3^{2-}	11	604.06	$\nu_4(PO_4^{3-})$
6	1096.8	$\nu_3(PO_4^{3-})$	12	569.93	$\nu_4(PO_4^{3-})$

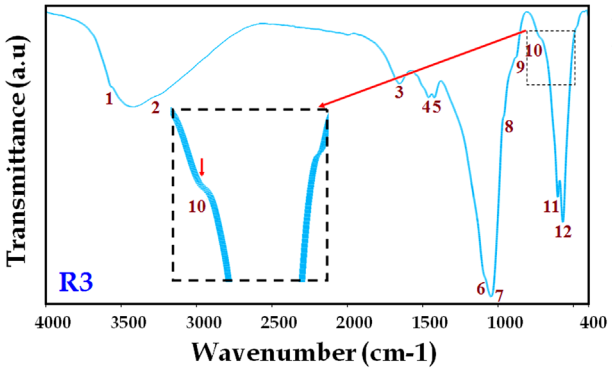

No.	cm^{-1}	Assignment	No.	cm^{-1}	Assignment
1	3565.8	OH^-	7	1045.65	$\nu_3(PO_4^{3-})$
2	3422.96	H_2O	8	960.45	$\nu_3(PO_4^{3-})$
3	1653.43	H_2O	9	884.71	CO_3^{2-}
4	1470.4	CO_3^{2-}	10	729.72	$P_2O_7^{4-}$
5	1422.02	CO_3^{2-}	11	603.19	$\nu_4(PO_4^{3-})$
6	1091.7	$\nu_3(PO_4^{3-})$	12	569.59	$\nu_4(PO_4^{3-})$

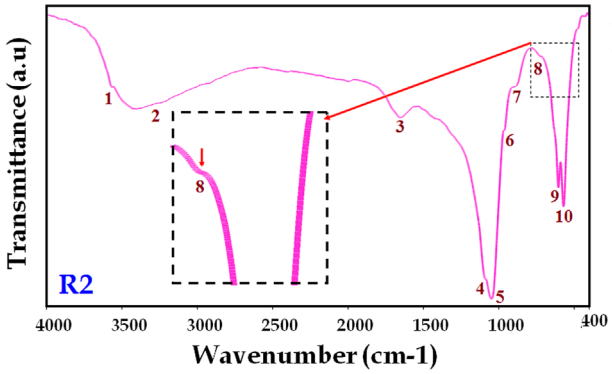

No.	cm^{-1}	Assignment	No.	cm^{-1}	Assignment
1	3565.8	OH^-	6	965.5	$\nu_1(PO_4^{3-})$
2	3403.28	H_2O	7	889.76	CO_3^{2-}
3	1657.10	H_2O	8	733.24	$P_2O_7^{4-}$
4	1091.7	$\nu_3(PO_4^{3-})$	9	603.99	$\nu_4(PO_4^{3-})$
5	1047.81	$\nu_3(PO_4^{3-})$	10	570.07	$\nu_4(PO_4^{3-})$

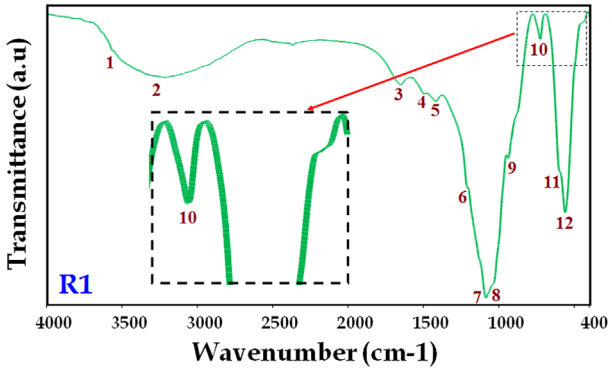

No.	cm^{-1}	Assignment	No.	cm^{-1}	Assignment
1	3570.8	OH^-	7	1089.54	$\nu_3(PO_4^{3-})$
2	3213.07	H_2O	8	1046.3	$\nu_3(PO_4^{3-})$
3	1662.3	H_2O	9	945.3	$P_2O_7^{4-}$
4	1515.8	CO_3^{2-}	10	729.72	$P_2O_7^{4-}$
5	1425	CO_3^{2-}	11	607.01	$\nu_4(PO_4^{3-})$
6	1212	$P_2O_7^{4-}$	12	564.68	$\nu_4(PO_4^{3-})$

Fig. 6. FT-IR spectra of R1, R2, R3 and R4 after 10 h of mechanical activation in M1 media.

in the FT-IR spectra of calcium phosphate-based materials are PO_4^{3-}, OH^-, CO_3^{2-}, and HPO_4^{2-} groups in the range 4000–400 cm^{-1}. The characteristic bands (listed in tables) exhibited in the milled powders for 10 h are assigned here:

(a) For the obtained powder out of R1, two bands were observed at 3213.07 cm^{-1} and 1662.3 cm^{-1} due to the vibration of the adsorbed water in the calcium phosphates [26]. These peaks shifted to 3403.28 cm^{-1} and 1657.10 cm^{-1} for R2, 3422.96 cm^{-1} and 1653.43 cm^{-1} for R3, and 3312.52 cm^{-1} and 1652.2 for R4. In addition, a weak peak at 3570.8 cm^{-1} belongs to the stretching vibration of lattice OH^- ions with small difference depending on the chemical compositions.

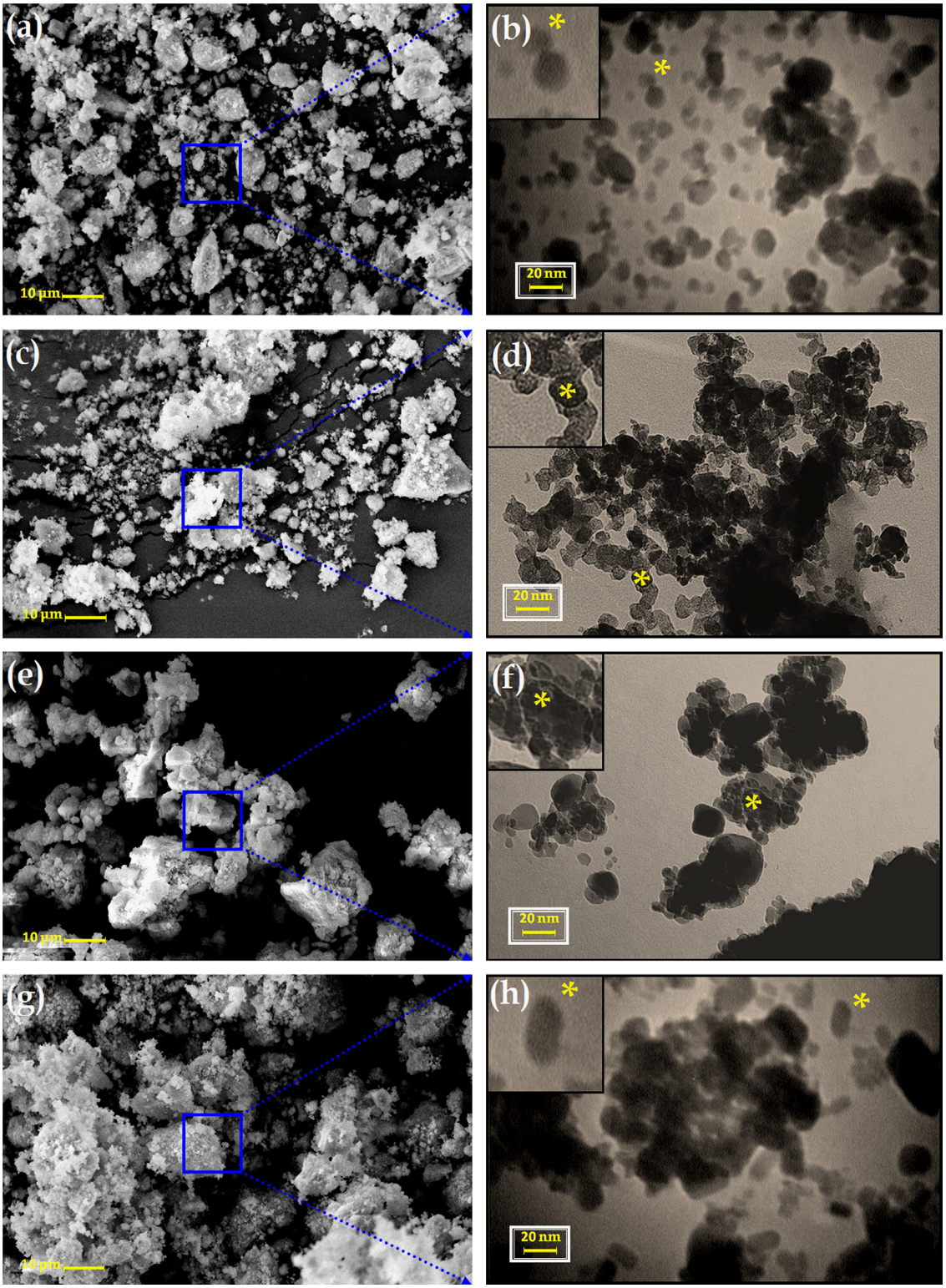

Fig. 7. SEM and TEM images of the outcomes of (a, b) R1, (c, d) R2, (e, f) R3 and (g, h) R4 after 10 h of mechanical activation in M1 media.

(b) In the case of R1, the bands at 1089.54 and 1046.3 cm^{-1} attributed to ν_3 PO_4, and the bands at 607.01 and 564.68 cm^{-1} result from ν_1 PO_4 [26,27]. These peaks shifted to 1091.7 cm^{-1}, 1047.81 cm^{-1}, 603.99 cm^{-1}, and 570.07 cm^{-1} for R2; 1091.7 cm^{-1}, 1045.65 cm^{-1}, 603.19 cm^{-1}, and 569.59 cm^{-1} for R3; and 1096.8 cm^{-1}, 1046.19 cm^{-1}, 604.06 cm^{-1}, and 569.93 cm^{-1} for R4. Also, besides the mentioned bands additional vibrations at 1212, 945.3 and 729.72 cm^{-1} appear for the R1. These vibrations correspond to pyrophosphate group ($P_2O_7^{-4}$) [28]. This result is in agreement with the XRD data which showed the characteristic peaks of calcium pyrophosphate.

It should be noted that these bands (except the band at 729.72 cm^{-1}) were not observed in other cases. However, the presence of weak band at 733.24 cm^{-1} for R2 and 729.72 cm^{-1} for R3 and R4 confirmed the existence of a small amount of calcium pyrophosphate in the products. It should be noted that the characteristic peaks of $Ca_2P_2O_7$ were not found in XRD profiles of R2, R3, and R4. The presence of $Ca_2P_2O_7$ could be assigned to the reactions occurring within the powder mixtures, which resulted in the formation of calcium pyrophosphate under the mechanical activation. The presence of pyrophosphate group in outcomes of R1, R2, R3, and R4 may be described by the following reactions:

$$2CaO+2H_2O \rightarrow 2Ca(OH)_2 \text{ (In the case of R1)} \quad (6)$$

$$2Ca(OH)_2+2H_3PO_4 \rightarrow Ca_2P_2O_7+5H_2O \quad (7)$$

$$CaO+2CaHPO_4 \rightarrow Ca_2P_2O_7+Ca(OH)_2 \text{ (In the case of R2)} \quad (8)$$

$$Ca(OH)_2+2H_3PO_4 \rightarrow Ca_2P_2O_7+5H_2O \text{ (In the case of R3)} \quad (9)$$

$$Ca(OH)_2+2CaHPO_4 \rightarrow Ca_2P_2O_7+CaO+2H_2O \text{ (In the case of R4)} \quad (10)$$

(c) For the obtained powder out of R1, a doublet appears at 1515.8 and 1425 cm^{-1} attributed to ν_3 vibration mode of the carbonated groups. These bands shifted to 1470.4 cm^{-1} and 1422.02 cm^{-1} for R3 and 1460.3 cm^{-1} and 1420 cm^{-1} for R4. In the case of R2, these bands were not found after 10 h of milling. In addition, a band at 889.76 cm^{-1} for R2, at 884.74 cm^{-1} for R3 and at 884.71 cm^{-1} for R4 attributed to ν_2 vibration mode of the carbonated groups. In general, the presence of these peaks showed that ATCP as the main phase of the milling process contained some CO_3^{2-} groups in PO_4^{3-} sites of apatite lattice (B-type substitution) [29]. According to the literature [30], this kind of calcium phosphate is more similar to biological apatite and could be more suitable for bone replacement materials.

According to FT-IR findings combined with XRD results, it can be concluded that the outcomes of R2, R3, and R4 had higher purity than the R1. In fact, these products exhibited combination of high phase and chemical purity that can be considered in biomedical applications.

3.5. Morphological characteristics (TEM and SEM observations)

Fig. 7 shows the SEM and TEM images of the outcomes of R1, R2, R3 and R4 after 10 h of mechanical activation in M1 media. According to this figure, the synthesized powders showed cluster-like structures which were comprised of several fine particles. The SEM observations indicated that the mean size of agglomerate was in the range of 1–5 μm. However, the distribution range of the agglomerates was not the same in different reactions. This behavior may be attributed to the coalescence of fine agglomerates/particles under mechanical activation. It is obvious that the obtained powder out of R1 in comparison with other samples showed less likely to agglomerate. It has been found [31], when two adjacent primary particles collide, the coalescence may take place on the premise that these two particles share a common crystallographic orientation. As a result, two primary particles attach to each other and combine into a secondary one. Since the sizes of the secondary particles are still very small, it is reasonable that they will continue to collide and coalesce which may ultimately lead to the agglomeration. A detailed microstructure information and morphology variation of the milled samples were further characterized by TEM. From TEM images, it can also be seen that the synthesized powders exhibited high tendency to agglomerate which is in agreement with SEM micrographs. In mechanically activated samples, this phenomenon corresponds to the nature of milling process which originates through repeated welding, fracturing and re-welding of fine powder particles [32]. According to TEM images (Fig. 7b and d), the obtained powders through R1 and R2 were composed of spheroidal particles in the nanometer regime (sub-100 nm). It has been found that nanoparticles with spherical morphology are better than other irregular morphologies due to the well space fillings and the low percentage of voids in the final product [26]. In addition, granules with a smooth spherical geometry have direct structural and functional connection with living bone that improve osseointegration [26,33]. The resultant powders out of R3 and R4 were comprised of ellipse-like particles with an average size of below 100 nm. According to the literature [34], nanostructured calcium phosphates with ellipse- or rod-like morphology inhibit the proliferation of malignant melanoma cells. In fact, these nanoparticles may be helpful to remedy cancer. Moreover, the products could be used as strength enhancing additives for the preparation of bionanocomposites.

Based on these observations, it can be concluded that the agglomeration tendency, average particle size and morphology of the n-ATCP are influenced by the chemical composition of reagents.

3.6. Thermal annealing process

Fig. 8 displays the XRD profile, FT-IR spectrum, SEM micrograph and TEM image of the product out of R1 after annealing at 1100 °C for 1 h. As shown in Fig. 8a, crystallization of amorphous phase occurred during heating at 1100 °C, and consequently high crystalline β-tricalcium phosphate (β-TCP) was generated. It should be mentioned that the extra peaks i.e. $Ca_2P_2O_7$ and CaO were not identified after thermal treatment and the only detected phase was β-TCP. This suggests that the synthesized powder had a high phase purity. Evaluation of the structural features after annealing indicated that the fraction of crystalline phase was significantly enhanced and reached 72% after thermal treatment at 1100 °C. It has been reported that calcium phosphates with high-level crystallinity are insoluble in physiological environment [25]. So the heat treated specimen can be considered for dental applications. Examination of the lattice parameters for the heat treated sample confirmed the formation of β-TCP. In accordance with the obtained data, the *a*-axis and *c*-axis values for the heat

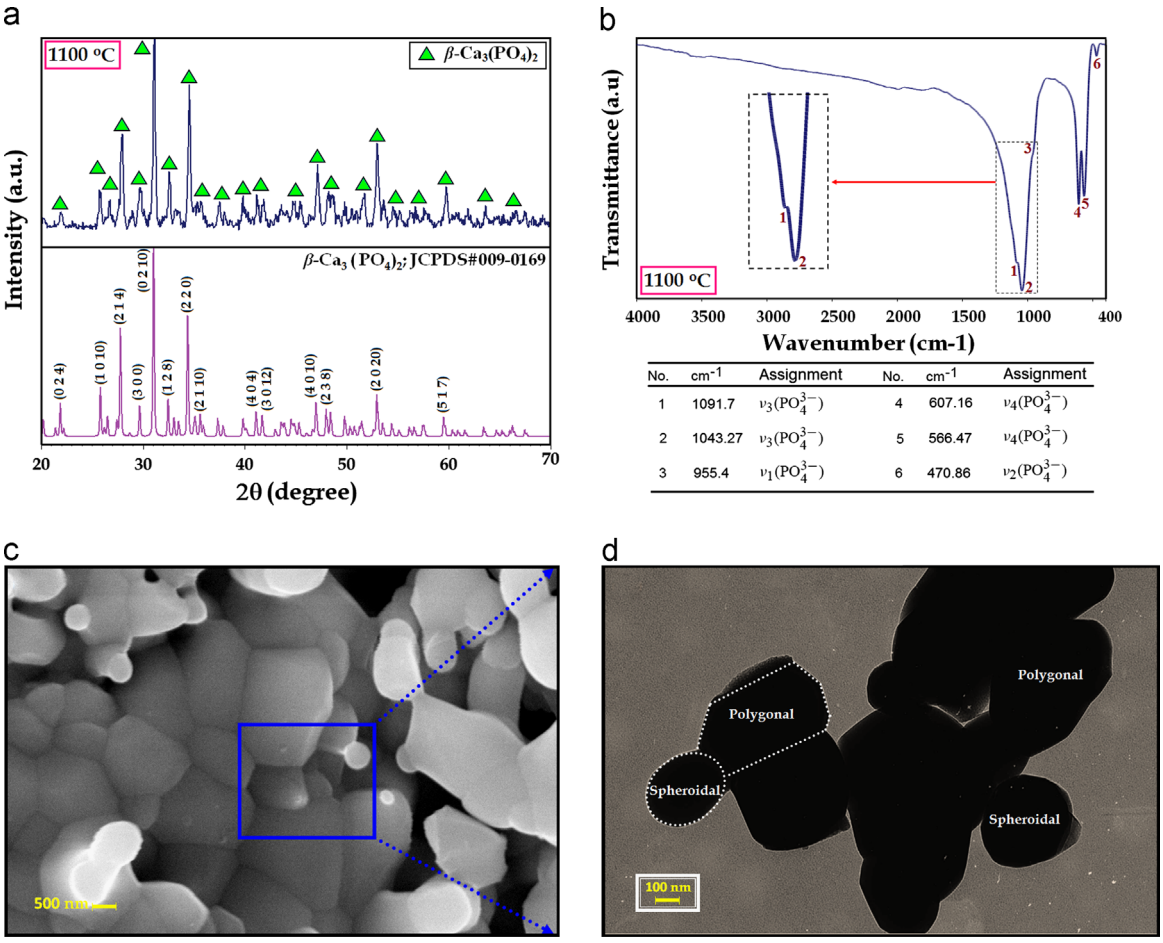

Fig. 8. (a) XRD profile, (b) FT-IR spectrum, (c) SEM micrograph, and (d) TEM image of the product out of R1 after annealing at 1100 °C for 1 h.

treated sample ($a=10.4065$ Å and $c=37.3989$ Å) were similar to the reported values for standard (#09-0169: $a=10.4290$ Å and $c=37.3800$ Å). However, the minor differences in crystal lattice characteristics can probably be attributed to the lattice distortion of β-TCP during the solid-state process. According to FT-IR spectrum Fig. 8b, two bands attributed to the vibration of the adsorbed water in the calcium phosphates and ν_3 vibration mode of the carbonated groups disappeared after thermal treatment at 1100 °C. In addition, the pyrophosphates characteristic bands was not visible in the case of sample thermally treated at 1100 °C. The annealed sample showed the characteristic peaks of β-TCP [28], in good agreement with the previous discussed results. In details, the peaks associated to the PO_4^{3-} were detected at 1091.7, 1043.27, 955.4, 607.16, 566.47, and 470.86 cm^{-1} accompanied by the disappearance of the hydroxyl group. Fig. 8c and d show the morphological features of the product out of R1 after annealing at 1100 °C for 1 h. These images clearly expose distinct differences in the microstructural characteristics of the samples. During heating at 1100 °C, grain growth occurred and the average particle size increased accordingly. Based on the TEM and SEM observations, the microstructure showed a bimodal grain size distribution characterized by the presence of coarse grains with a mean size of around 2 μm along with finer grains with an average size of about 300 nm.

4. Conclusions

Mechanosynthesis of amorphous tricalcium phosphate nanopowders using different raw materials was investigated. Results showed that the milling time, media type and chemical composition of raw materials had significant effects on the formation of nano-sized amorphous tricalcium phosphate. After 5 h of milling, the main product of mechanical activation for both milling media was amorphous tricalcium phosphate. In metallic vial using un-fused alumina balls, mechanical activation to 10 h led to the formation of extra phase due to the excessive adhesion of balls to the milling media. The crystallinity degree decreased and reached a minimum after 10 h of mechanical activation in both milling vials. On the other hand, the XRD findings combined with FT-IR results revealed that the purity of mechanosynthesized amorphous tricalcium phosphate nanopowders was considerably influenced by the chemical composition of reagents. Based on SEM and TEM observations, the synthesized powders tended to agglomerate during the solid-state process. However, the level of agglomeration was not the same in different specimens. After annealing at 1100 °C, the microstructure showed a bimodal grain size distribution characterized by the presence of coarse grains with a mean size of around 2 μm along with finer grains with an average size of about 300 nm.

Acknowledgment

The authors are grateful to research affairs of Islamic Azad University, Najafabad Branch for supporting of this research.

References

[1] C. Combes, C. Rey, Amorphous calcium phosphates: synthesis, properties and uses in biomaterials, Acta Biomaterialia 6 (2010) 3362–3378.
[2] W.J. Dunn, Shear bond strength of an amorphous calcium phosphate-containing orthodontic resin cement, American Journal of Orthodontics and Dentofacial Orthopedics 131 (2007) 243–247.
[3] S. Somrania, M. Banub, M. Jemalc, C. Rey, Physico-chemical and thermochemical studies of the hydrolytic conversion of amorphous tricalcium phosphate into apatite, Journal of Solid State Chemistry 178 (2005) 1337–1348.
[4] S.V. Dorozhkin, Amorphous calcium (ortho)phosphates, Acta Biomaterialia 6 (2010) 4457–4475.
[5] A. Lebugle, E. Zahidi, G. Bonel, Effect of structure and composition on the thermal decomposition of calcium phosphates (Ca/P = 1.33), Reactivity of Solids 2 (1986) 151–161.
[6] P. Layrolle, A. Lebugle, Characterization and reactivity of nanosized calcium phosphates prepared in anhydrous ethanol, Chemistry of Materials 6 (1994) 1996–2004.
[7] A. Rodrigues, A. Lebugle, Behavior in wet atmosphere of an amorphous calcium phosphate with an atomic Ca/P ratio of 1.33, Journal of Solid State Chemistry 148 (1999) 308–315.
[8] J.C. Heughebaert, G. Montel, Conversion of amorphous tricalcium phosphate into apatitic tricalcium phosphate, Calcified Tissue International 34 (1982) S103–S108.
[9] H.E. Lundager Madsen, I. Lopez-Valero, V. Lopez-Acevedo, R. Boistelle, The formation of amorphous tricalcium phosphate at 37 °C, Journal of Crystal Growth 75 (1986) 429–434.
[10] E.D. Eanes, I.H. Gillessen, A.S. Posner, Intermediate states in the precipitation of hydroxyapatite, Nature 208 (1965) 365–367.
[11] N.C. Blumenthal, A.S. Posner, Effect of preparation conditions on the properties and transformation of amorphous calcium phosphate, Materials Research Bulletin 7 (1972) 1181–1189.
[12] J.E. Harries, D.W.L. Hukins, C. Holt, S.S. Hasnain, Conversion of amorphous calcium phosphate into hydroxyapatite investigated by EXAFS spectroscopy, Journal of Crystal Growth 84 (1987) 563–570.
[13] E.D. Eanes, Thermochemical studies on amorphous calcium phosphate, Calcified Tissue Research 5 (1970) 133–145.
[14] T. Yu, J. Ye, Y. Wang, Synthesis and property of a novel calcium phosphate cement, Journal of Biomedical Materials Research Part B: Applied Biomaterials 90B (2009) 745–751.
[15] A. Tofighi, R. Palazzolo, Calcium phosphate bone cement preparation using mechano-chemical process, Key Engineering Materials 284–286 (2005) 101–104.
[16] U. Gbureck, O. Grolms, J.E. Barralet, L.M. Grover, R. Thull, Mechanical activation and cement formation of β-tricalcium phosphate, Biomaterials 24 (2003) 4123–4131.
[17] U. Gbureck, J.E. Barralet, L. Radu, H. Klinger, R. Thull, Amorphous α-tricalcium phosphate: preparation and aqueous setting reaction, Journal of the American Ceramic Society 87 (2004) 1126–1132.
[18] S.N. Vaidya, V. Sugandhi, Pressure induced amorphization in calcium phosphates, Journal of Materials Science 34 (1999) 3769–3778.
[19] E. Boanini, M. Gazzano, A. Bigi, Ionic substitutions in calcium phosphates synthesized at low temperature, Acta Biomaterialia 6 (2010) 1882–1894.
[20] A.S. Posner, F. Betts, Synthetic amorphous calcium phosphate and its relation to bone mineral structure, Accounts of Chemical Research 8 (1975) 273–281.
[21] C. Suryanarayana, Mechanical alloying and milling, Progress in Materials Science 46 (2001) 1–184.
[22] F. Sun, F.H.S. Froes, Synthesis and characterization of mechanical-alloyed Ti_xMg alloys, Journal of Alloys and Compounds 340 (2002) 220–225.
[23] S.S. Rayalu, J.S. Udhoji, S.U. Meshram, R.R. Naidu, S. Devotta, Estimation of crystallinity in flyash-based zeolite-A using XRD and IR spectroscopy, Current Science 89 (2005) 2147–2151.
[24] T. Nakano, A. Tokumura, Y. Umakoshi, Variation in crystallinity of hydroxyapatite and the related calcium phosphates by mechanical grinding and subsequent heat treatment, Metallurgical and Materials Transactions A 33 (2002) 521–528.
[25] K.P. Sanosh, M.C. Chu, A. Balakrishnan, Y.J. Lee, T.N. Kim, S.J. Cho, Synthesis of nano hydroxyapatite powder that simulate teeth particle morphology and composition, Current Applied Physics 9 (2009) 1459–1462.
[26] B. Nasiri-Tabrizi, A. Fahami, R. Ebrahimi-Kahrizsangi, Effect of milling parameters on the formation of nanocrystalline hydroxyapatite using different raw materials, Ceramics International 39 (2013) 5751–5763.
[27] S. Nath, R. Tripathi, B. Basu, Understanding phase stability, microstructure development and biocompatibility in calcium phosphate–titania composites, synthesized from hydroxyapatite and titanium powder mixture, Materials Science and Engineering C 29 (2009) 97–107.
[28] I. Cacciotti, A. Bianco, High thermally stable Mg-substituted tricalcium phosphate via precipitation, Ceramics International 37 (2011) 127–137.
[29] J.P. Lafon, E. Champion, D. Bernache-Assollant, Processing of AB-type carbonated hydroxyapatite $Ca_{10-x}(PO_4)_{6-x}(CO_3)_x(OH)_{2-x-2y}(CO_3)_y$ ceramics with controlled composition, Journal of the European Ceramic Society 28 (2008) 139–147.
[30] M.H. Fathi, E. Mohammadi Zahrani, Mechanical alloying synthesis and bioactivity evaluation of nanocrystalline fluoridated hydroxyapatite, Journal of Crystal Growth 311 (2009) 1392–1403.
[31] A. Fahami, B. Nasiri-Tabrizi, R. Ebrahimi-Kahrizsangi, Synthesis of calcium phosphate-based composite nanopowders by mechanochemical process and subsequent thermal treatment, Ceramics International 38 (2012) 6729–6738.
[32] B. Nasiri-Tabrizi, A. Fahami, R. Ebrahimi-Kahrizsangi, Current microscopy contributions to advances in science and technology, in: A. Méndez-Vilas (Ed.), Characterization of Nanostructured Calcium Phosphate-Based Bioceramics: TEM and SEM/FE-SEM Studies, Formatex, Spain, 2012, pp. 1259–1270.
[33] B. Nasiri-Tabrizi, P. Honarmandi, R. Ebrahimi-Kahrizsangi, P. Honarmandi, Synthesis of nanosize single-crystal hydroxyapatite via mechanochemical method, Materials Letters 63 (2009) 543–546.
[34] P. Honarmandi, P. Honarmandi, A. Shokuhfar, B. Nasiri-Tabrizi, R. Ebrahimi-Kahrizsangi, Milling media effects on synthesis, morphology and structural characteristics of single crystal hydroxyapatite nanoparticles, Advances in Applied Ceramics 109 (2010) 117–122.